Institute for Advanced Technology
The University of Texas at Austin

IAT

Cavity Dynamics for Long Rod Penetration

Minhyung Lee and Stephan Bless
Institute for Advanced Technology
The University of Texas at Austin

January 1996

IAT.R 0094

Certification of Technical Review

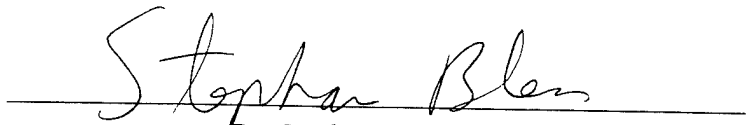

Dr. Stephan Bless

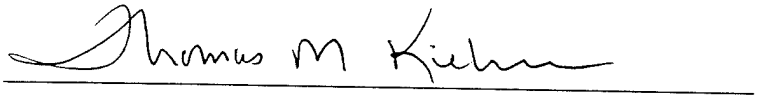

Dr. Thomas Kiehne

REPORT DOCUMENTATION PAGE

Form Approved
OMB NO. 0704-0188

1. AGENCY USE ONLY (Leave blank)	2. REPORT DATE	3. REPORT TYPE AND DATES COVERED
	January 1996	Technical Report, OCT 1995 - DEC 1995

4. TITLE AND SUBTITLE

Cavity Dynamics for Long Rod Penetration

5. FUNDING NUMBERS

Contract # DAAA21-93-C-0101

6. AUTHOR(S)

M. Lee and S. Bless

7. PERFORMING ORGANIZATION NAME(S) AND ADDRESS(ES)

Institute for Advanced Technology
The University of Texas at Austin
4030-2 W. Braker Lane, #200
Austin, TX 78759

8. PERFORMING ORGANIZATION REPORT NUMBER

IAT.R 0094

9. SPONSORING / MONITORING AGENCY NAME(S) AND ADDRESS(ES)

U.S. Army Research Laboratory
ATTN: AMSRL-WT-T
Aberdeen Proving Ground, MD 21005-5066

10. SPONSORING / MONITORING AGENCY REPORT NUMBER

11. SUPPLEMENTARY NOTES

The view, opinions and/or findings contained in this report are those of the author(s) and should not be considered as an official Department of the Army position, policy, or decision, unless so designated by other documentation.

12a. DISTRIBUTION / AVAILABILITY STATEMENT

Approved for public release; distribution unlimited.

12b. DISTRIBUTION CODE

A

13. ABSTRACT *(Maximum 200 words)*

Two analytical models for the crater size due to long rod penetrations are presented. The energy method is the first which, in a steady state penetration, relates the kinetic energy loss of a penetrator to the total energy deposited in the target. An equation of cavity dynamics is set up by assuming a radial motion in the target. This approach appears to provide an upper bound of the crater size due to the neglect of energy losses in the penetrator. The second method is based on the observations that two mechanisms are involved in cavity growth due to long rod penetrators: flow of penetrator erosion products, which exerts radial stress on the target and opens a cavity, and axial inertia of the target as it flows around the penetrator nose. The analysis includes the centrifugal force exerted by the penetrator, radial inertia of the target, and the strength of the target. Thus, the extent of cavity growth due to penetrator mushrooming, which cannot be predicted by other analyses, can be estimated. The analytical models are compared with existing formulas and empirical equations and found to be more accurate than other analyses in the literature. Numerical calculations using AUTODYN-2D are also conducted and these confirm the phenomenological assumptions in the models.

14. SUBJECT TERMS

crater size, long-rod penetration, equation of cavity dynamics, centrifugal force, target inertia, penetrator mushrooming

15. NUMBER OF PAGES

14

16. PRICE CODE

17. SECURITY CLASSIFICATION OF REPORT	18. SECURITY CLASSIFICATION OF THIS PAGE	19. SECURITY CLASSIFICATION OF ABSTRACT	20. LIMITATION OF ABSTRACT
Unclassified	Unclassified	Unclassified	UL

Contents

List of Figures

List of Tables

Cavity Dynamics for Long Rod Penetration

Minhyung Lee and Stephan Bless

ABSTRACT

Two analytical models for the crater size due to long rod penetrations are presented. The energy method is the first which, in a steady state penetration, relates the kinetic energy loss of a penetrator to the total energy deposited in the target. An equation of cavity dynamics is set up by assuming a radial motion in the target. This approach appears to provide an upper bound of the crater size due to the neglect of energy losses in the penetrator.

The second method is based on the observations that two mechanisms are involved in cavity growth due to long rod penetrators: flow of penetrator erosion products, which exerts radial stress on the target and opens a cavity, and axial inertia of the target as it flows around the penetrator nose. The analysis includes the centrifugal force exerted by the penetrator, radial inertia of the target, and the strength of the target. Thus, the extent of cavity growth due to penetrator mushrooming, which cannot be predicted by other analyses, can be estimated.

The analytical models are compared with existing formulas and empirical equations and found to be more accurate than other analyses in the literature. Numerical calculations using AUTODYN-2D are also conducted and these confirm the phenomenological assumptions in the models.

I. INTRODUCTION

The cavity dynamics and the resulting crater size created by long rod, kinetic energy (KE), anti-armor penetrators are examined analytically and numerically.

The radial motion of target material generated by hypervelocity penetration occurs in two stages as shown in numerical simulations [1]. In the first stage, eroded penetrator elements play the dominant role in opening a cavity. In the second stage, the inertia deposited in the target is responsible for the further cavity expansion until the strength of the target forces it to come to rest.

An earlier analytical study of the crater size from long rod penetrators is presented by Szendrei [2] based upon a momentum argument. By accounting for the first stage with a proper choice of initial conditions, Shinar et al. [3] set up an equation for processes occurring during the second stage and determined the final crater size. However, there are some difficulties associated with the initial conditions, since they assume that the inertia phase starts when the cavity radius is equal to the initial penetrator radius. Based on an energy balance argument, Tate [4] provided an approximate formula for the crater diameter. Bjerke et al. [5] presented an empirical equation for the channel diameter versus impact velocity by fitting a polynomial to data for tungsten-nickel-iron sintered penetrators ranging from 90 to 94% tungsten impacting thick and normal incidence steel targets.

In the present work, we propose two analytical models for the crater size. The analytical models are compared with existing formulas and empirical equations. An energy method states that the kinetic energy of a penetrator is converted to the plastic work for crater production and kinetic energy deposited in the target. This approach can provide the upper bound of the cavity size due to the neglect of energy absorbed during deformation of the penetrator.

The second model uses the method of Miller [6] to determine the amount of the first stage cavity expansion due to eroded penetrator element. Because of the neglect of the target strength in his model, the cavity radius is not bounded. In the present work, including the strength of the target allows us to explore the ultimate cavity radius achieved during the first stage cavity expansion, due solely to a mushrooming effect. We then use the energy method in order to estimate the amount of the second stage cavity expansion due to inertia.

In both models, an axisymmetric coordinate system moving at the constant penetration velocity U is used as reference. Numerical simulations using AUTODYN-2D are also presented in comparison with the analytical predictions.

II. ENERGY PRINCIPLES

The mathematical formulation of the cavity dynamics for penetration of long rod penetrators is described in this section within the framework of an energy balance principle. The basic assumptions required in the analyses are:

- Target material is considered as incompressible and inviscid.
- The motion of the cavity wall is purely radial.
- The internal energy change due to thermal effects and strain energy in the target are negligible.
- Energy absorbed by the projectile is negligible.
- Steady state is assumed.
- The penetrator material ultimately comes to rest.

A. Kinetic Energy Loss of a Penetrator Per Unit Target Length

Consider a long rod penetrator of density ρ_p, diameter D_p, and length L impacting an infinite target of density ρ_t at normal incidence. For a penetrator with an impact velocity V, the kinetic energy loss of the penetrator per unit target length is given by,

$$E_{kP} = \frac{1}{2}\left(\frac{m}{P}\right)V^2 , \qquad (1)$$

where $m = \rho_p (\pi r_p^2)$. Here m is the mass, P the final penetration depth and r_p the

radius of the penetrator. Using the hydrodynamic relation $L/P=(V-U)/U$, where U is the penetration velocity, Eq. (1) becomes,

$$E_{kP} = \frac{1}{2}\rho_p(\pi r_p^2)\,\frac{(V-U)}{U}\,V^2 . \tag{2}$$

With this result, an energy balance equation will be set up for the purpose of determining an equation of cavity dynamics.

B. Equation of Cavity Dynamics

It is assumed that the kinetic energy loss of the penetrator per unit target length equals the total energy deposited in the target (kinetic energy plus plastic work done to open a cavity). If the radial velocity is u(r), then following [7], the source strength is related to the radial distance r,

$$u = \varsigma / r . \tag{3}$$

The kinetic energy per unit target length E_{kt} in the radial field within a finite radius Ω is then,

$$E_{kt} = \int_a^{\Omega} (\pi\rho_t\, u^2 r)\, dr = \pi\rho_t\varsigma^2\, N , \tag{4}$$

where, $N = \ln(\Omega/a)$ is a dimensionless geometric parameter and a is a cavity radius. If we replace Ω by na and n is assumed to vary in the range 5-15, N can be treated as a constant. In the calculation N equals 2.3. The amount of plastic work done to open the cavity per unit target length is given by,

$$E_{pt} = \int_0^{a} (2\pi r)\, R_t\, dr = \pi a^2\, R_t , \tag{5}$$

where R_t is the target resistance for radial cavity expansion. Now the conservation of the energy per unit target length can be expressed by the relation.

$$E_{kp} = \pi\rho_t\varsigma^2\, N + \pi a^2\, R_t . \tag{6}$$

By introducing constants,

$$P^2 = \frac{E_{kp}}{\pi R_t}, \qquad Q^2 = \frac{R_t}{\rho_t N} , \tag{7}$$

we can obtain an expression for the source strength given by,

$$\varsigma = Q\sqrt{P^2 - a^2} . \tag{8}$$

In Eq. (3), the source strength is also $a\dot{a}$. In order to obtain the equation of cavity dynamics, Eqs. (3) and (8) are combined to give,

$$a\dot{a} = Q\sqrt{P^2 - a^2} \quad . \tag{9}$$

Integration of Eq. (9) with a boundary condition $a\,(t = 0) = 0$ yields,

$$a(t) = \sqrt{P^2 - (P - Qt)^2} \quad . \tag{10}$$

Equation (10) determines the time evolution of the cavity radius. The cavity has a maximum at time, $t_{max} = P/Q$. Note that Eq. (10) is valid only for $0 < t < t_{max}$. At t_{max}, the velocity field vanishes throughout the flow field so the kinetic energy in the target becomes zero. The maximum cavity radius is then equal to,

$$a_c(t_{max}) = P = \sqrt{\frac{E_{kp}}{\pi R_t}} \quad . \tag{11}$$

By substituting Eq. (2), we have ,

$$a_c = r_p\sqrt{\frac{\frac{1}{2}\rho_p V^2}{R_t}\,\frac{(V - U)}{U}} \quad . \tag{12}$$

A similar formula to Eq. (12) can be determined from momentum principles and given by (Appendix A),

$$a_c = r_p\sqrt{\frac{Y_p}{R_t} + \frac{2\rho_p(V - U)^2}{R_t}} \quad , \tag{13}$$

where Y_p is the dynamic yield strength of the penetrator. Tate's formula [4] obtained from an energy balance argument is,

$$a_c = r_p\sqrt{1 + \frac{2\rho_p(V - U)^2}{R_t}} \quad . \tag{14}$$

If U=V/2 and $2\rho_p(V - U)^2 / R_t \geq 1$, this equation coincides with Eq. (12). Equation (13) has the same form as Eq. (14) but with 1 replacing Y_p / R_t. Although Eqs. (12), (13) and (14) are similar in form, they are derived from different arguments. Equations (12) and (14) are based upon transformation of penetrator kinetic energy to work done during cavity expansion and Eq. (13) is based upon momentum exchange between the penetrator and target. These equations will be compared quantitatively in the comparison section.

C. Determination of the Penetration Velocity (U)

For steady state penetration the modified Bernoulli equation applies,

$$\frac{1}{2}\rho_p(V-U)^2 + Y_p = \frac{1}{2}\rho_t U^2 + R_t \,. \tag{15}$$

Then U is given by [4],

$$U = \frac{V - \alpha\sqrt{V^2 + 2(1-\alpha^2)(R_t - Y_p)/\rho_t}}{(1-\alpha^2)}\,, \tag{16}$$

where $\alpha = \sqrt{\rho_t / \rho_p}$. The theoretical R_t value determined by the classical spherical cavity expansion model as presented by Satapathy and Bless [8] is used in the present work:

$$R_t = -\frac{2}{3}Y \ln\left(\frac{Y}{2G}\right) + \frac{2}{3}Y \,, \tag{17}$$

which gives for RHA steel the value $R_t = 5.0$ GPa.

In Figure 1, the present model prediction for the evolution of the cavity radius is compared with experimental results for copper jets obtained by de Rosser and Merendino [9] and the analytical results given by Shinar et al. [3]. The impact velocity was 7.6 km/s and r_p was taken to be 1.75 mm. The yield stress of their steel target was taken to be 0.8 GPa. It can be seen that the agreement between the present model and experiments is excellent for the evolution period.

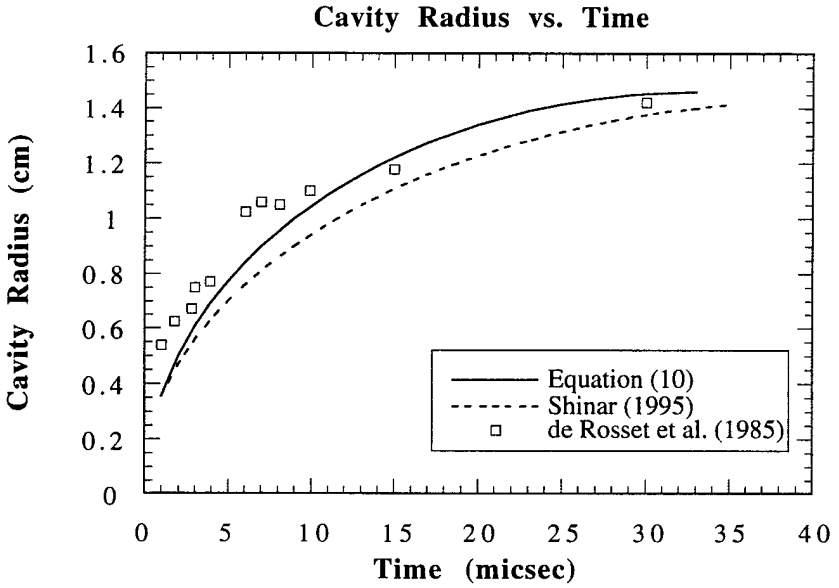

Figure 1. Evolution of the cavity formed in RHA steel.

III. TWO STAGE CAVITY EXPANSION MODEL (TSCEM)

We propose that in the first stage, the eroded penetrator elements exert pressure on the target and open a cavity. In the second stage, the inertia imparted to the target is responsible for the further expansion of the cavity, especially during hypervelocity penetration. It is hypothesized that the final cavity radius is equal to the sum of the cavity radii produced by each stage acting independently, regardless of the order of application of loads. In other words, we use the principle of superposition for the total work done by each stage. The analysis includes the centrifugal force exerted by the penetrator, radial inertia of the target, and the strength of the target. The basic assumptions required in the analysis are:

- Target material is considered as incompressible, steady inviscid flow relative to the stagnation region.
- The pressure profile exerted by the target is assumed to be $\frac{1}{2}\rho_t U^2 \sin^3\beta$ as provided in Ref. [6], where β is the angle between the tangent direction of the centerline and the axis of symmetry. Although the Newtonian pressure, $\frac{1}{2}\rho_t U^2 \sin^2\beta$, allows a simple closed-form solution, it over-predicts the pressure profile [6]. This pressure is acting normal to the flow at radius r, where r is the radius of the centerline of an eroded projectile element.
- The stagnation region over which the pressure equals $\frac{1}{2}\rho_t U^2$ exists for $\frac{1}{2} \le \beta \le \pi$. The domain for the outside of the stagnation region is $0 \le \beta \le \pi/2$.
- For the inertia calculation, we make an analogy with the case of a rigid body penetrator. This is due to the fact that a projectile head moving at constant velocity U induces a kinetic energy transfer to the target. For simplicity, the energy method described in the previous model is then adopted.

A. First Stage Cavity Expansion

With these assumptions, the first stage cavity expansion can be derived from Miller's analysis [6] with presence of the strength of the target. The target strength will eventually halt the cavity growth. The geometry of the first stage cavity expansion is shown in Figure 2.

From mass conservation in a coordinate system located at the penetration front, the thickness of the eroded projectile element is given by,

$$\tau(\beta) = \frac{r_p^{\,2}}{2r(\beta)} . \tag{18}$$

Since the pressure force is acting normal to the flow at radius r, the centrifugal forces in the eroded element for the outside of the stagnation region must be balanced by the resistance which is equal to the pressure force plus the strength of the target,

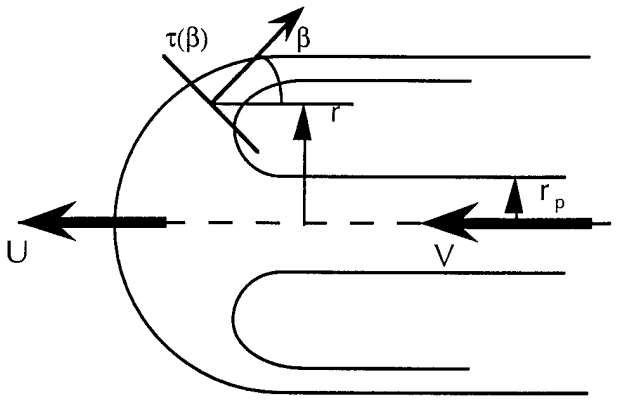

Figure 2. Geometry of the first stage cavity expansion model.

$$R_t + \frac{1}{2}\rho_t U^2 \sin^3\beta = \tau(\beta)\,\rho_p \frac{(V-U)^2}{R(\beta)}, \tag{19}$$

where $R(\beta)$ is the scaled local radius of curvature of the center line curve. R_t in this equation is approximately an average of the spherical and cylindrical cavity expansion stresses. From geometric relations,

$$R(\beta) = -\frac{1}{\sin\beta}\frac{dr}{d\beta}, \tag{20}$$

Combining Eqs. (18), (19) and (20) gives the differential equation describing the trajectory of an eroded projectile element given by,

$$R_t + \frac{1}{2}\rho_t U^2 \sin^3\beta = -\frac{r_p^{\,2}}{2r}\rho_p (V-U)^2 \sin\beta \left(\frac{dr}{d\beta}\right)^{-1}. \tag{21}$$

By introducing two constants,

$$S = \frac{\frac{1}{2}\rho_p (V-U)^2}{R_t}, \qquad T = \frac{\frac{1}{2}\rho_t U^2}{R_t}. \tag{22}$$

Eq. (21) becomes,

$$2r\,dr = -\frac{2r_p^{\,2}\,S\sin\beta}{1+T\sin^3\beta}\,d\beta. \tag{23}$$

In order to determine the trajectory of the eroded element as a function of β, this equation is to be integrated with an initial condition, $r(\beta = \pi/2) = r_1$ which yields,

$$r(\beta) = \sqrt{r_1^2 - \int_{90}^{\beta} \frac{2r_p^2 S \sin\beta}{1+T\sin^3\beta}\, d\beta} \,. \tag{24}$$

By integrating Eq. (24) numerically for the entire domain of $0 \le \beta \le \pi/2$, we can determine the final crater size (a_{c1}). Miller [6] made a hypothesis that there is a stagnation region in which the pressure is equal to $\frac{1}{2}\rho_t U^2$, such that $r_1/r_p > 1$. Note that if the target pressure is approximated to be $\frac{1}{2}\rho_t U^2 \sin^2\beta$, there is a simple closed-form solution given by,

$$a_{c1} = r_p \sqrt{\left(\frac{r_1}{r_p}\right)^2 + \frac{S}{\sqrt{T+T^2}} \ln\left[\, 1+2T+2\sqrt{T+T^2} \,\right]} \,. \tag{25}$$

In order to find the initial condition r_1, by the same reasoning used above, Eq. (19) can be written inside of the stagnation region as,

$$R_t + \frac{1}{2}\rho_t U^2 = \tau(\beta)\, \rho_p \frac{(V-U)^2}{R(\beta)} \,. \tag{26}$$

Again by using the radius of curvature and the thickness of the elements, this equation is to be integrated with an initial condition $r(\beta = -\pi/2) = r_p/2$, which yields,

$$r_1 = r_p \sqrt{\frac{1}{4} + \frac{2S}{1+T}} \,. \tag{27}$$

B. Second Stage Cavity Expansion

In addition to first stage cavity expansion due to centrifugal forces exerted by the eroded penetrator elements, the inertia imparted to the target is responsible for further cavity expansion. This inertia is created by flow in the target around a penetrator head moving at constant velocity U. In order to estimate the additional cavity expansion due to target inertia, we consider target response to an "equivalent penetrator"- a rigid body of the same shape penetrator head and the same penetration velocity. We can then use the energy method described previously.

Consider a rigid penetrator moving through the target with Poncelet resistance. Then the force (energy per unit target length) may be written as follows,

$$F = A + BU^2 \,, \tag{28}$$

where,

$$A = (\pi a_{c1}^2) R_t, \qquad B = 1/2(\pi a_{c1}^2) C_d \rho_t \ . \tag{29}$$

Here C_d is the drag coefficient. In these equations, A is the target resistance force associated with plastic work and B is the drag force which comes about due to the convective inertia effects. For the second stage, this inertia is responsible for the cavity expansion from a_{c1} to a_c. Hence,

$$\frac{1}{2}(\pi a_{c1}^2) C_d \rho_t U^2 = \int_{a_{c1}}^{a_c} 2\pi r R_t dr = \pi \left(a_c^2 - a_{c1}^2\right) R_t \ . \tag{30}$$

The solution to the final crater size is then given by,

$$a_c = a_{c1} \sqrt{1 + \frac{\frac{1}{4} \rho_t U^2}{R_t}} \ . \tag{31}$$

The drag coefficient is assumed to be 0.5 for a hemispherical nose. The extent of the compensation due to inertia increases with impact velocity because the U^2 term in Eq. (31) becomes more important in the high impact velocity limit.

IV. NUMERICAL SIMULATIONS

Numerical simulations of tungsten long rod projectiles (L/D=10) into infinite RHA steel targets were conducted using an AUTODYN-2D finite difference code. The objective of the simulations was to confirm the phenomenological assumptions made in the analytical models, and to compare numerical results to the analytical results. We use a constant shear modulus G and a von-Mises yield surface with a yield strength Y as shown in Table I.

Table I. Shear Stress Parameters

	Steel	Tungsten
G (GPa)	120	140
Y (GPa)	1.2	2

AUTODYN is an Eulerian wave propagation code allowing for a maximum grid of 60,000 cells. The Mie-Gruniesen equation of state (E.O.S.) is used for both materials. The parameters are the same as in Ref. [10] and listed in Table II.

In all runs a constant subgrid with eight cells across the radius of the projectile and continuing for three diameters away from the projectile is used. The penetration direction has a constant cell size to make the subgrid a 1:1 aspect ratio.

Table II. E.O.S. Parameters

	Steel	Tungsten Alloy
ρ_o(g/cc)	7.86	17.4
C_o (km/s)	3.57	4.03
S	1.92	1.26
Γ_o	1.7	1.7
P_{min} (GPa)	-2.	-2.

V. COMPARISON OF ANALYTICAL, NUMERICAL, AND EXPERIMENTAL RESULTS

The crater diameters normalized by the projectile diameter obtained from the analytical and experimental results versus impact velocities are shown in Figure 3. The results are compared with the numerical predictions obtained by using AUTODYN-2D with eight cells across the radius. The numerical simulations slightly underestimate the crater size, which is also found in the work of Bjerke, et al. [5].

As shown in Figure 3, the results obtained from the first stage cavity expansion analysis is rather good until V>2 km/s. This is due to the fact that the inertia effects become important in this range. However, the analysis can provide the extent of the mushrooming versus impact velocity. By including inertia in the two stage cavity expansion model, the analytical predictions compare well to the data.

It should be emphasized that the model based on energy conservation provides an upper bound for the final crater size because energy losses due to penetrator deformation are ignored. That is, it is assumed that all of the available kinetic energy of the projectile is used to open the cavity. It can be shown that Eqs. (12) and (14) match Tate's formula quite well in the high velocity range but the Tate's formula appears to over-predict crater size in the low impact velocity range. The agreement between the energy and momentum models is quite good. The equations for the crater diameter obtained from different methods are shown in Appendix B.

VI. CONCLUSIONS

Two analytical models for the crater diameter formed by long rod penetrations are presented and compared with existing formulas and empirical equations.

An advantage of the energy principle is that it can provide an upper bound for the crater size. It can also provide the evolution of the cavity radius. The formula from the momentum principle appears to provide good agreement with experiments despite the crudeness of the model.

An estimation of the amount of mushrooming with respect to impact velocity is a valuable contribution of this analysis. Maximum penetration for a given kinetic energy should occur

with a reduction of the mushrooming, reading to a smaller resistance force, as discussed by Magness and Farrand [11].

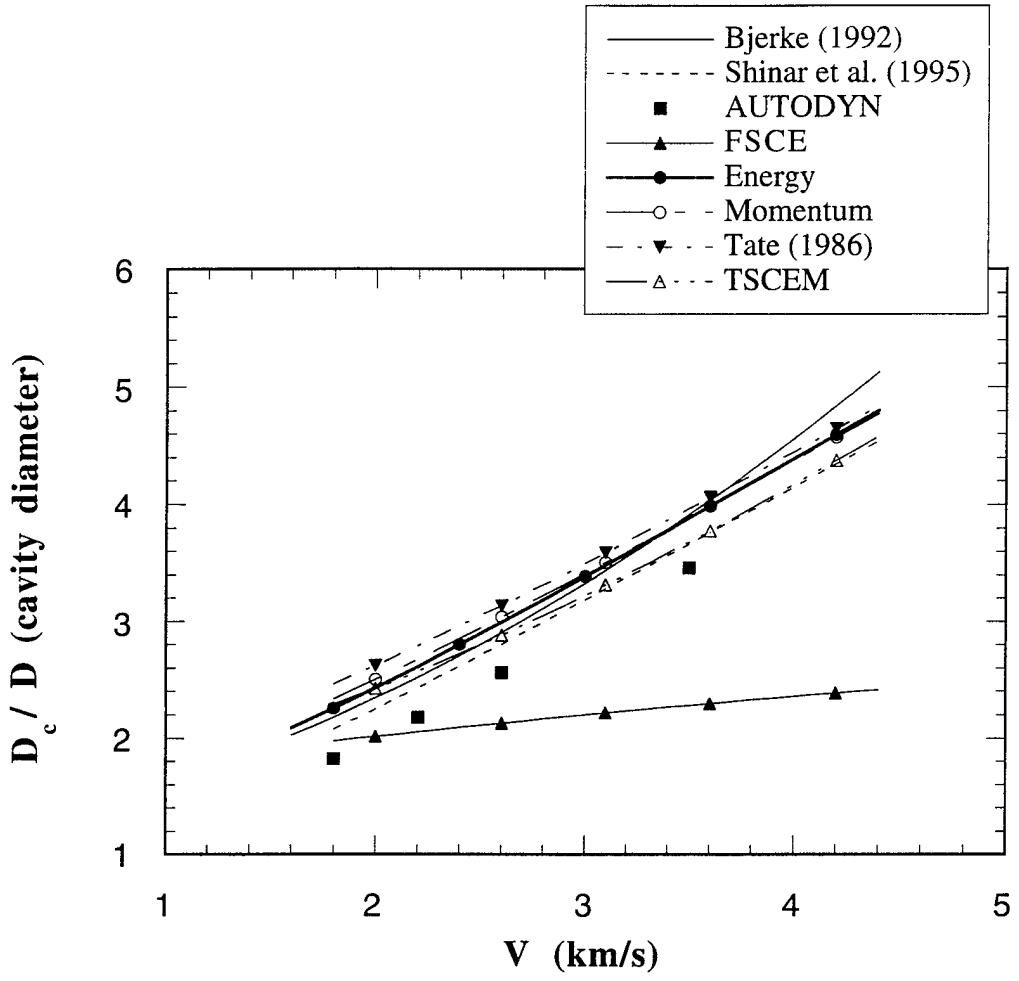

Figure 3. Ratio of cavity diameter to rod diameter versus impact velocity. Tungsten alloy striking RHA steel target. FSCE represents the results from the first stage cavity expansion. AUTODYN represents results obtained with the AUTODYN wavecode. Models are summarized in Appendix B.

REFERENCES

[1] Y. Kivity and E. Hirsch, "Penetration Cutoff Velocity for Ideal Jets," Ballistics' 87, 10th Int. Symp., San Diego, CA., 1987.

[2] T. Szendrei, "Analytical Model for Crater Formation by Jet Impact and Its Application on Penetration Curves and Profiles," Ballistics' 83, 7th Int. Symp., Hague, 1983.

[3] G. I. Shinar, N. Barnea, M. Ravid and E. Hirsch, "An Analytical Model for the Cratering of Metallic Targets by Hypervelocity Long Rods," Ballistics' 95, 15th Int. Symp., Israel, 1995.

[4] A. Tate, "Long Rod Penetration Models - Part II. Extensions to the Hydrodynamic Theory of Penetration," *Int. J. Mech. Sci.*, vol. 28, no. 9, pp. 599-612, 1986.

[5] T. W. Bjerke, G. F. Silsby, D. R. Scheffler and R. M. Mudd, "Yawed Long-Rod Armor Penetration," *Int. J. Impact Engng.*, vol. 12, no. 2, pp. 281-292, 1992.

[6] C. W. Miller, "Two-Dimensional Engineering Model of Jet Penetration," Ballistics' 95, 15th Int. Symp., Israel, 1995.

[7] Y. Partom, "Does Target Resistance to Long Rod Penetration Decrease with Increasing Impact Velocity?," IAT. R0028, August 1993.

[8] S. Satapathy and S. Bless, "Quasi-Static Penetration Tests of PMMA: Analysis of Strength and Crack Morphology," submitted for publication to *J. Mech. Mat'ls.*, 1995.

[9] W. S. De Rosset and A. B. Merendino, "Radial Hole Growth: Experiment vs. Calculation," Ballistics' 85, 8th Int. Symp., Orlando, FL., 1995.

[10] Y. Partom, "Projectile-Flow Effect for Long Rod Penetration," Ballistics' 95, 15th Int. Symp., Israel, 1995.

[11] L. S. Magness and T. G. Farrand, "Deformation Behavior and Its Relationship to the Penetration Performance of High-Density KE Penetrator Materials," Proc. of 1990 Army Science Conference, May 1990.

APPENDIX A

MOMENTUM PRINCIPLES

Consider long rod penetration into a homogeneous target. A control volume attached to the penetration interface of two bodies is shown in Figure A. The control volume is bounded on the left by the penetration interface, on the right by the Hugoniot elastic-plastic interface, and on the top and bottom by the material interfaces. The penetration interface is moving with velocity U. Mass enters the control volume through the elastic plastic interface. To determine the final cavity size approximately, the conservation of momentum equation for the control volume is,

$$2\rho_p(\frac{\pi}{4}D^2)(V-U)^2 + Y_p(\frac{\pi}{4}D^2) = \int_0^{a_c} R_t(2\pi r)dr = R_t(\frac{\pi}{4}D_c^{\,2}) \ , \qquad \text{(A1)}$$

where D_c is the crater diameter and R_t is the radial cavity expansion stress. The conservation of mass equation for the control volume is introduced into this equation by equating the incoming mass to the outgoing mass in a steady state condition. The solution for the final crater diameter is then given by,

$$\left(\frac{D_c}{D}\right)^2 = \frac{Y_p}{R_t} + \frac{2\rho_p(V-U)^2}{R_t} \ . \qquad \text{(A2)}$$

If Y_p / R_t is replaced by one, this expression coincides with Tate's formula (Eq. (14)).

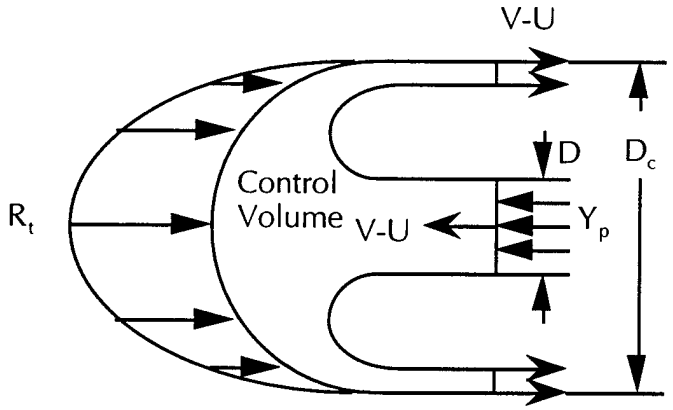

Figure A. Control Volume

APPENDIX B

EQUATION OF CRATER SIZE

Energy principle:

$$a_c = r_p \sqrt{\frac{\frac{1}{2}\rho_p V^2}{R_t} \frac{(V - U)}{U}} \quad . \tag{12}$$

Momentum principle:

$$a_c = r_p \sqrt{\frac{Y_p}{R_t} + \frac{2\rho_p (V - U)^2}{R_t}} \quad . \tag{13}$$

Tate [4]:

$$a_c = r_p \sqrt{1 + \frac{2\rho_p (V - U)^2}{R_t}} \quad . \tag{14}$$

TSCEM:

$$a_c = a_{c1} \sqrt{1 + \frac{\frac{1}{4}\rho_t U^2}{R_t}} \quad , \tag{31}$$

$$a_{c1} = r_p \sqrt{\frac{1}{4} + \frac{2S}{1+T} + \int_0^{90} \frac{2S \sin\beta}{1 + T \sin^3\beta} \, d\beta} \quad . \tag{B1}$$

Szendrei [2]:

$$a_c = r_p \sqrt{\frac{V^2}{2Y_p\left(1/\sqrt{\rho_p} + 1/\sqrt{\rho_t}\right)}} \quad . \tag{B2}$$

Shinar et al. [3]:

$$a_c = r_p \sqrt{1 + \frac{\sqrt{3}\, V^2}{4Y_p\left(1/\sqrt{\rho_p} + 1/\sqrt{\rho_t}\right)}} \quad . \tag{B3}$$

Bjerke et al. [5]:

$$a_c = r_p\left(1.1524 + 0.3388V + 0.1286V^2\right) . \tag{B4}$$

Distribution List

Administrator
Defense Technical Information Center
Attn: DTIC-DDA
8725 John J. Kingman Road, Ste 0944
Ft. Belvoir, VA 22060-6218

Director
US Army Research Lab
ATTN: AMSRL OP SD TA
2800 Powder Mill Road
Adelphi, MD 20783-1145

Director
US Army Research Lab
ATTN: AMSRL OP SD TL
2800 Powder Mill Road
Adelphi, MD 20783-1145

Director
US Army Research Lab
ATTN: AMSRL OP SD TP
2800 Powder Mill Road
Adelphi, MD 20783-1145

Army Research Laboratory
AMSRL-CI-LP
Technical Library 305
Aberdeen Prvg Grd, MD 21005-5066

Dr. Marv Alme
Alme & Associates
PO Box 764
Columbia, MD 21045

Dr. Charles Anderson, Jr.
Southwest Research Institute
Engineering Dynamics Department
P.O. Box 28510
San Antonio, TX 78228-0510

Joseph E. Backofen
Brigs Co.
2668 Petersborough St.
Herndon, VA 22071-2443

T. Bjerke
Director
U.S. Army Research Laboratory
Attn: AMSRL-WT-TC
Aberdeen Prvg Grd, MD 21005-5066

Mr. Carl F. Cline
Physicist
Lawrence Livermore National La
L-017
P.O. Box 808
Livermore, CA 94550

Randolph S. Coates
US Army Research Laboratory
AMSRL-WT-TC
APG, MD 21005-5066

Andrew Crowson
U.S. Army Research Office
P.O. Box 12211
Research Triangle Park, NC 27709-2211

W. deRosset
U.S. Army Research Laboratory
Attn: AMSRL-WT-TC
Aberdeen Prvg Grd, MD 21005-5066

Doug Elder
Kaman Sciences Corporation
1500 Garden of the Gods Road
P.O. Box 7463
Colorado Springs, CO 80933-7463

Mr. William Flis
Dyna East Corporation
3201 Arch St.
Philadelphia, PA 19104

Mr. Michael Forrestal
Sandia National Laboratory
Division 1922
P.O. Box 5800
Albuquerque, NM 87185

Dr. Joe Foster
Air Force Armament & Technology Lab
AFATL/MNW
Eglin AFB, FL 32542

K. Frank
U.S. Army Research Laboratory
Attn: AMSRL-WT-TD
Aberdeen Prvg Grd, MD 21005-5066

Marilyn Freeman
Liaison Officer
SARD-TR Room 3E 480
Research, Development and Acquisition
103 Army Pentagon
Washington, D.C. 20310-0103

Mr. Tom Furmaniak
TACOM
U.S. Army Tank and Auto Command
AMSTA-JSK
Warren, MI 48397-5000

W. J. Gillich
U.S. Army Research Laboratory
AMSRL-WT-TA
Aberdeen Prvg Grd, MD 21005-5066

Distribution List

Tim Holmquist
Alliant Techsystems, Inc.
Twin City Army Ammunition Plant-Bldg. 103
New Brighton, MN 55112

Thomas L. Menna
General Research Corporation
5383 Hollister Ave.
Santa Barbara, CA 93111

George Snyder
U.S. Army Missile Command
Attn: AMSMI-RD-ST-WF
Redstone Arsenal, AL 35898-5247

Dr. William Isbell
ATA Associates
P. O. Box 6570
Santa Barbara, CA 93111

Dr. Walter Morrison
Chief, Terminal Effects Division
U.S. Army Research Laboratory
Aberdeen Prvg Grd, MD 21005-5066

Dr. Joseph Sternberg
Physics Dept.
Naval Postgraduate School
Monterey, CA 93943

Dr. Thomas Kiehne
Institute for Advanced Technology
The University of Texas at Austin
4030-2 W. Braker Lane, Suite 200
Austin, TX 78759

Peter Nebolsine
Physical Sciences, Inc.
20 New England Bus. Ctr
Andover, MA 01810

Robert J. Taylor
Lockheed Martin Vought Systems
M/S: WT-21
P.O. Box 650003
Dallas, TX 75265-0003

Mr. Rene Larriva
Interferometrics Corporation
8150 Leesburg Pike, Suite 1400
Vienna, VA 22182-2799

Mr. Dennis L. Orphal
The Titan Corporation
California Research & Technology Division
5117 Johnson Drive
Pleasanton, CA 94566

James L. Thompson
U.S. Army Tank-Automotive Research,
Development and Engineering Center
Attn: AMSTA-JS
Warren, MI 48397-5000

Dr. Hartmuth F. Lehr
Institute Saint Louis
5, Rue du General Cassagnou
Boite Postal 34
F-68301 Saint Louis, CEDEX
FRANCE

Martin N. Raftenberg
US Army Research Lab
AMSRL-WT-TD
APG, MD 21005-5066

Jerome D. Yatteau
Principal Engineer
Applied Reseach Associates
Suite 305
7114 West Jefferson Ave.
Lakewood, CO 80235-2309

Nick Lynch
DERA Fort Halstead
Bldg. A 20, Div. WX5
Sevenoaks, Kent
England TN14 7BP

A. M. Rajendran
US Army Research Lab
Arsenal St.
Watertown, MA 02172

William Marley
U.S. Army Nat'l Ground Intelligence Ctr
IANG-RMT
220 Seventh Street, N.E.
Charlottesville, VA 22901-5396

Edward Schmidt
U.S. Army Research Laboratory
Attn: AMSRL-WT-PB
Aberdeen Prvg Grd, MD 21005-5066